Revista Internacional de Métodos Numéricos para Cálculo y Diseño en Ingeniería

Sensitivity improvement to eddy current displacement sensor in full maglev LVAD

Wenfei Tao[1], Chen Chen[1]

1 Artificial Organ Technology Laboratory, School of Mechanical and Electrical Engineering, Soochow University, Suzhou 215000, China

Abstract

Eddy current displacement sensors in full-maglev left ventricular assist devices (LVADs) suffer from low sensitivity resulting from the use of a stator titanium alloy frame. The aim of this study was to develop a methodology to improve the sensitivity of eddy current displacement sensors and formulate a mathematical model of coil impendence to illustrate the impact of the addition of a titanium alloy frame between the sensor coils and the measured conductor. An equivalent mutual inductance model in the circuit was established for LVADs with and without a titanium alloy frame stator wall. Comparing the differences in excitation frequency and measured metal conductivity considering the relation of inductance with displacement enabled the development of methods to improve the sensitivity of the sensor when a titanium frame is added to the stator. An experiment was conducted to collect and analyze data to ascertain the relation between impedance and rotor displacement considering different excitation frequencies, stators with and without a titanium alloy frame, and the copper ring. Relatively high sensitivity was acquired when titanium frames of 0.25-mm thickness were applied to both the stator and rotor with an additional copper ring attached to the rotor frame at an excitation frequency of 475 kHz.

OPEN ACCESS

Published: 08/11/2023

Accepted: 23/10/2023

DOI:
10.23967/j.rimni.2023.10.006

Keywords:
Eddy current displacement sensor
titanium alloy frame
impendence
left ventricular assist device (LVAD)
magnetic bearing

1. Introduction

The full maglev left ventricular assist device (LVAD) is among the most effective replacement methods for heart transplant treatment to treat heart failure. The core component of an LVAD is the magnetic bearing system. It typically consists of a displacement sensor and an electromagnet. Owing to their high robustness, eddy current displacement sensors are widely used as displacement sensors in magnetic bearing systems. It is a type of magnetic micro-distance displacement sensor with a detection coil and a measured conductor added. Considering the biocompatibility requirements of LVAD systems, a titanium alloy frame is added between the coil and the measured metal in the LVAD. This design reduces the sensitivity of the eddy current sensor and even changes its impedance, which results in higher power consumption and reduced stability in the magnetic bearing system.

Oberle et al. [1] designed a small type of eddy current sensor that featured low power consumption (10 mW) and low cost for use in magnetic bearing systems. The low power consumption made the sensor suitable for implantable life-support systems. Fang et al. [2] designed an eddy current sensor with a dual-probe coil and a multiple-channel structure to increase its linearity range. Wang et al. [3] designed an eddy current displacement sensor with better bandwidth, higher resolution, and strong robustness to improve pump performance in an active magnetic bearing. Chi et al. [4] studied the use of a titanium alloy frame in the stator, pure titanium added to the rotor, and a coil excitation frequency of 2 MHz in the eddy current displacement sensor. Ahn et al. [5] designed a specific sensor of small size for an axial-flow maglev LVAD and conducted studies on its nonlinear characteristics and temperature drift. Lee et al. [6] designed an eddy current displacement sensor used in axial LVADs with 500 kHz of excitation frequency; the titanium alloy in the stator was only 0.15 mm thick. The sensor outer diameter was 2.38 mm, with 0.88-mm thickness, 190 turns of coils, and 0.04-mm wire diameter. Sun et al. [7] designed a new eddy current sensor with low circuit complexity, high linearity, and high sensitivity. This design contributed significantly to the sensor's mass production. Nagaoka et al. [8] achieved two-degrees-of-freedom control for a magnetic bearing through three eddy current sensors and applied this design to a centrifugal blood pump. Raghunathan et al. [9] introduced a low-cost commercial digital eddy current sensor with a resolution up to 7 μm. Zhan et al. [10] analyzed the impact of surface curvature and eccentric distance on eddy current sensor measurement. The measurement error was eccentrically compensated and they improved the radial position accuracy in the magnetic bearing system.

In recent years, patient physiology has required better blood pump designs with smaller sizes. Achieving the goal of designing smaller but smarter pumps entails new challenges for adopting displacement sensors for full-maglev LVADs. Eddy current displacement sensors are optimal options for small full-maglev LVADs. However, few studies have addressed the impact of the titanium alloy frame on the eddy current sensor performance, and few studies have provided a clear demonstration of its impedance. The aim of this study was to establish a mathematical model of the coil impedance for an eddy current displacement sensor with a stator titanium frame. This mathematical model was used to demonstrate the sensor sensitivity with different excitation frequencies. Compared with traditional eddy current sensors without a stator metal frame, this type is more complex and sensitive to the excitation frequency. An optimal combination was determined using this

Correspondence: Wenfei Tao (taowenfeitt@163.com).

method, which helps to improve the engineering design.

2. Mathematical model of the sensor with a stator frame

When high-frequency voltage and current signals are excited in sensor coils, eddy current losses occur on the surface of the measured conductor in response to the change in distance between the coils and the measured conductor; the coil impedance is also affected by this change. This is the working principle of eddy current displacement sensors. However, for LVADs, which are implantable and designed to remain in the body for many years, a titanium alloy frame must be used between the rotor and sensor coil for biocompatibility. The frame causes large changes in the eddy current displacement sensor. A displacement sensor with low sensitivity and signal-to-noise ratio directly exhibits a decrease in its stability and increase in power consumption for the magnetic bearing system, which restrains the LVAD performance.

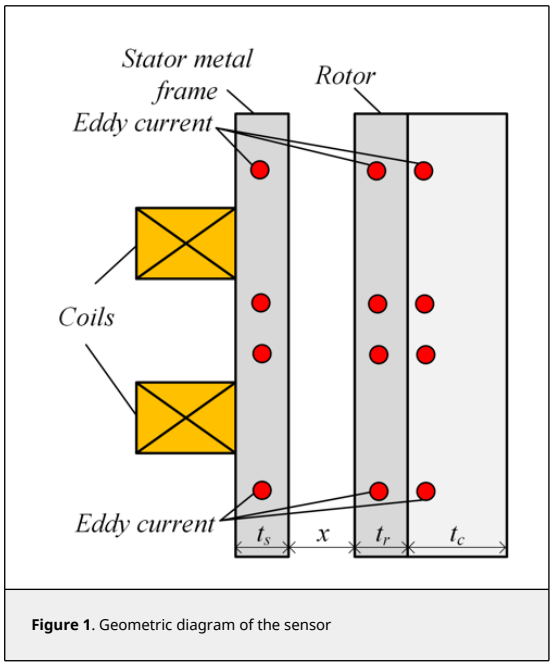

Figure 1. Geometric diagram of the sensor

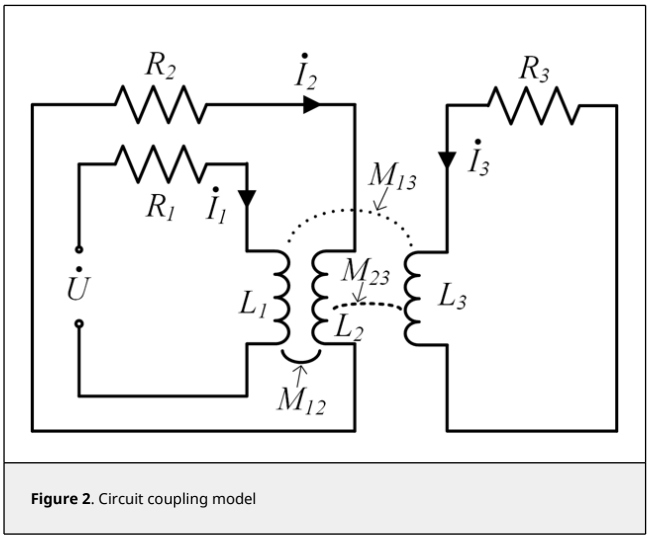

Figure 2. Circuit coupling model

Figure 1 shows a section drawing of the sensor coil, stator metal frame, and rotor. t_r is the frame thickness of the rotor, t_s is the frame thickness of the stator, and t_c is the thickness of the rotor filler. When the filler is metal, it creates an eddy current on its surface. x is the displacement between stator and rotor, as shown in Figure 1. The rotor surface can be used as the basis for displacement sensor detection as long as it is a conductive metal. The phasor model of the three loops shown in Figure 2 are expressed as

$$\begin{aligned}(j\omega L_1 + R_1)\dot{I}_1 - j\omega M_{12}\dot{I}_2 - j\omega M_{13}\dot{I}_3 &= \dot{U}\\ j\omega M_{12}\dot{I}_1 - j\omega M_{23}\dot{I}_3 - (j\omega L_2 + R_2)\dot{I}_2 &= 0\\ j\omega M_{13}\dot{I}_1 - j\omega M_{23}\dot{I}_2 - (j\omega L_3 + R_3)\dot{I}_3 &= 0\end{aligned} \quad (1)$$

where ω refers to the coil excitation frequency, L_1 refers to the self-inductance of the sensor coil, R_1 refers to the internal resistance of the sensor coil, $\dot{I}_1$ refers to the phase current of loop 1, L_2 refers to the self-inductance of the eddy current ring in the stator frame, R_2 refers to the internal resistance of the eddy current ring in the stator metal frame, $\dot{I}_2$ refers to the phase current of loop 2, $\dot{I}_3$ refers to the phase current of loop 3, L_3 refers to the self-inductance of the eddy current ring in the rotor, R_3 refers to the internal resistance of the rotor eddy current ring, M_{12} refers to the mutual inductance of the sensor coil and the stator metal frame, M_{13} refers to the mutual inductance between the sensor coil and rotor eddy current ring, M_{23} refers to the mutual inductance between the eddy current ring of the stator and rotor, and $\dot{U}$ refers to the sensor coil phase voltage.

Assuming that no stator metal frame is added, $L_2 = R_2 = M_{23} = M_{12} = \dot{I}_2 = 0$ the impedance of loop 1 can be written as

$$Z_{13} = \left(R_1 + \frac{\omega^2 M_{13}^2}{R_3^2 + \omega^2 L_3^2} R_3\right) + j\omega\left(L_1 - \frac{\omega^2 M_{13}^2}{R_3^2 + \omega^2 L_3^2} L_3\right). \quad (2)$$

Eq. (2) shows the equivalent impedance of a traditional eddy current displacement sensor; the real part of this equation represents equivalent resistance, and the imaginary part of this equation shows the equivalent inductance. M_{13} is inversely proportional to the distance between sensor coil and rotor, that is, the mutual inductance is 0 when the rotor is at infinity to the sensor coil. However, a decrease in distance causes a greater loss of eddy current, higher equivalent resistance, and lower equivalent inductance in the coils. In conclusion, the distance between the eddy current sensor coil and the measured conductor is inversely proportional to its equivalent resistance and directly proportional to its equivalent inductance, and its excitation frequency is directly proportional to its sensitivity in a traditional eddy current displacement sensor.

Similarly, when a metal frame is added to the stator, and there is no rotor, it acquires $L_3 = R_3 = M_{23} = M_{13} = \dot{I}_3 = 0$, and the impedance of loop 1 can be written as

$$Z_{12} = \left(R_1 + \frac{\omega^2 M_{12}^2}{R_2^2 + \omega^2 L_2^2} R_2\right) + j\omega\left(L_1 - \frac{\omega^2 M_{12}^2}{R_2^2 + \omega^2 L_2^2} L_2\right). \quad (3)$$

Eq. (3) refers to the impedance between the sensor coil and the stator metal frame. The value of M_{12} is not variable by the constant distance between the sensor coil and stator metal frame, when the frame thickness is determined. The flux from the eddy current ring on the surface of the stator metal frame always counteracts the flux created by the sensor coil. Therefore, the metal frame added to the stator directly affects sensor sensitivity. A thinner stator metal frame provides better

performance.

When both the stator metal frame and rotor frame are fully considered, $M_{23}\dot{I}_3$ can be completely neglected in the second subset of Eq. (1), considering that the induced electromotive force generated by the sensor coil to the stator metal frame is much higher than that generated by the rotor to the stator metal frame. The impedance of sensor coil can be written as

$$Z_{123} = (R_1 + \frac{\omega^2 M_{12}^2}{R_2^2 + \omega^2 L_2^2} R_2 + \frac{\omega^2 M_{13}^2}{R_3^2 + \omega^2 L_3^2} R_3 - \frac{\omega^4 M_{12} M_{13} M_{23} (R_3 L_2 + R_2 L_3)}{(R_2^2 + \omega^2 L_2^2)(R_3^2 + \omega^2 L_3^2)}) + j\omega (L_1 - \frac{\omega^2 M_{12}^2}{R_2^2 + \omega^2 L_2^2} L_2 - \frac{\omega^2 M_{13}^2}{R_3^2 + \omega^2 L_3^2} L_3 - \frac{\omega^2 M_{12} M_{13} M_{23} (R_2 R_3 - \omega^2 L_2 L_3)}{(R_2^2 + \omega^2 L_2^2)(R_3^2 + \omega^2 L_3^2)}). \quad (4)$$

The mutual inductance at each position in Eq. (4) is

$$M_{12} = k_{12}(d_{12})\sqrt{L_1 L_2}, \quad (5)$$

$$M_{23} = k_{23}(d_{23})\sqrt{L_2 L_3}, \quad (6)$$

$$M_{13} = k_{13}(d_{13})\sqrt{L_1 L_3}, \quad (7)$$

where $k_{12}(d_{12}), k_{13}(d_{13}), k_{23}(d_{23})$ are coupling coefficients, d_{12} is the mean geometric distance between the sensor coil and the eddy current ring on the stator metal frame, d_{13} is the mean geometric distance between the sensor coil and the eddy current ring on rotor, d_{23} is the mean geometric distance between the eddy current ring on stator metal frame and on rotor. The coupling coefficient indicates that the inductance is inversely proportional to the mean geometric distance, and the value of $k_{12}(d_{12}), k_{13}(d_{13}), k_{23}(d_{23})$ ranges from 0 to 1. The computation of the coupling coefficient is a complicated process, and details are not included in this paper.

When assigning a relatively high excitation frequency to the sensor coil, it acquires $R_i^2 \ll \omega^2 L_i^2, i = 1, 2, 3, R_2 R_3 \ll \omega^2 L_2 L_3$, and Eqs. (5)–(7) can be substituted into Eq. (4) as follows:

$$Z_{123} = [R_1 + k_{12}^2(d_{12}) L_1 R_2/L_2 + k_{13}^2(d_{13}) L_1 R_3/L_3 - L_1 k_{12}(d_{12}) k_{13}(d_{13}) k_{23}(d_{23})(R_2/L_2 + R_3/L_3)] + j\omega L_1 [1 - k_{12}^2(d_{12}) - k_{13}^2(d_{13}) + k_{12}(d_{12}) k_{13}(d_{13}) k_{23}(d_{23})]. \quad (8)$$

Similarly, the impedance of the sensor coil without adding the stator frame can be written as

$$Z_{13} = [R_1 + k_{13}^2(d_{13}) L_1 R_3/L_3] + j\omega L_1 [1 - k_{13}^2(d_{13})]. \quad (9)$$

Because the excitation frequency and metal conductivity affect the geometric size of the eddy current ring on the metal surface, the skin depth of the metal conductors and x (rotor displacement) are contained in d_{13} and d_{23}. The skin depth of the measured conductor surface can be calculated as

$$h = \sqrt{\frac{2}{\omega \sigma \mu}}, \quad (10)$$

where σ refers to the measured metal conductivity, and μ refers to permeability. $k_{12}(d_{12}), k_{13}(d_{13}), k_{23}(d_{23})$ is inversely proportional to the mean geometric distance, which is directly proportional to excitation frequency ω and conductivity σ. That is, a higher excitation frequency or conductivity of measured metal will lead to stronger coupling when the eddy current ring is closer to the sensor coil.

The thickness of the stator metal frame is much smaller than its skin depth to ensure that the magnetic field of the sensor coil can sense the rotor displacement; however, the actual thickness of the stator metal frame is affected by the manufacturing capability. When the thickness of the stator metal frame and the relative position between the sensor coil and stator metal frame are both determined, the above-mentioned coupling coefficients can be rewritten as $k_{12}(\sigma, \omega)$, $k_{13}(\sigma, x, \omega)$, $k_{23}(\sigma, x, \omega)$. $k_{12}(\sigma, \omega)$ changes as the stator metal frame conductivity and excitation frequency change in a directly proportional manner:

$$k_{12}(\sigma, \omega), k_{13}(\sigma, x, \omega), k_{23}(\sigma, x, \omega) \propto \sigma, \omega$$

$$k_{13}(\sigma, x, \omega), k_{23}(\sigma, x, \omega) \propto 1/x < .$$

When the coil inductance is considered as the basis of reference for the rotor displacement, the sensor sensitivity is defined as the derivative of the coil equivalent inductance on the rotor displacement. Then, by comparing the ratios of the sensitivity between stators with and without a metal frame, the equation can be written as

$$Sy = \frac{\partial(1 - k_{12}^2(\sigma, \omega) - k_{13}^2(\sigma, x, \omega) + k_{12}(\sigma, \omega) k_{13}(\sigma, x, \omega) k_2}{\partial(1 - k_{13}^2(\sigma, x, \omega))/\partial x} \quad (11)$$

$$= 1 - \frac{1}{2} k_{12}(\sigma, \omega)[\frac{k_{23}(\sigma, x, \omega)}{k_{13}(\sigma, x, \omega)} + \frac{\partial k_{23}(\sigma, x, \omega)}{\partial k_{13}(\sigma, x, \omega)}$$

The following conclusions are derived from Eqs. (4)–(11):

1. k_{12} indicates the coupling between the sensor coil and the stator metal frame; the sensitivity of the sensor decreases under any condition with a stator metal frame compared to that without the stator metal frame. When k_{12} is 0, no coupling occurs, which means that no metal frame is added to the stator. The variation of k_{23} is smaller than k_{12} and k_{13}, it can be considered as a fixed value.
2. When the excitation frequency increases, the coupling between the sensor coil and stator metal frame is also improved, but the stator metal frame has greater loss to the magnetic field of the sensor coil (i.e., k_{12} increases). Meanwhile, the coupling between the rotor and sensor coil also increases with frequency (i.e., k_{13} increases). The sensor sensitivity does not increase as the excitation frequency improves, although an optimal frequency exists that ensures the highest sensitivity in a sensor with a stator metal frame. The excitation frequency is defined on the basis of the metal frame thickness and conductivity. Considering the skin depth of the frame, the excitation frequency should not be set too high.
3. The combination of a stator metal frame with low conductivity and a rotor with high conductivity is beneficial for improving the sensor sensitivity. For LVADs, although titanium alloy has a relatively lower conductivity than copper or aluminum, the rotor and stator surfaces must be titanium. The application of a metal a with high conductivity beneath the titanium alloy frame of a rotor improves its integral conductivity, allowing a low-frequency magnetic field to penetrate the rotor titanium alloy frame.
4. The real part of impedance Z_{123} should be subtracted by a coupled item. When there is strong coupling between the sensor coil and stator metal frame, the resistance change of the coil caused by eddy current loss might not be directly proportional to the intensity of the mutual inductance. That is, when the excitation frequency is high, the equivalent resistance of the sensor coil increases as the distance between the rotor and sensor coil increases, which is completely opposite to the traditional regulation.

5. The imaginary part of impedance Z_{123} is different from that of traditional regulation. The last item shows that the gradient of the equivalent inductance is damped, unlike that in the traditional regulation. Fortunately, compared with the equivalent resistance of the sensor coil, it does not reverse the monotonicity of the equivalent inductance with displacement owing to the relation shown in $-k_{12}^2 - k_{13}^2 \leq -2k_{12}k_{13} \leq -k_{12}k_{13}k_{23}$, $0 \leq k_{12}, k_{13}, k_{23} \leq 1$.

3. Experiment

Titanium alloy was used for the stator and rotor frame, considering the LVAD biocompatibility requirements. However, the conductivity of titanium alloys is relatively low. The titanium alloy frame on the stator and rotor must be as thin as possible to increase the sensitivity of the eddy current sensor. In addition, copper was added beneath the rotor titanium frame to improve the conductivity. The parameters are shown in Table 1.

Table 1. Frame parameters

Stator thickness t_T	Rotor thickness t_S	Copper ring thickness t_C	Titanium alloy conductivity	Copper conductivity
0.25 mm	0.25 mm	0.65 mm	0.7 MS/m	57 MS/m

To verify the mathematical model and the above-mentioned conclusions, Table 2 lists the experimental groups for different configurations of stator frame, rotor frame, and copper ring. The rotor displacement x ranged from −0.25 mm to +0.25 mm. The −0.25 mm value represents the nearest position between rotor and sensor coil, and +0.25 mm is the farthest position. In this case, the measurement step size of rotor displacement was 0.05 mm. The excitation frequency was set from 100 to 1000 kHz, and the step size was set to 25 kHz. The equivalent resistance and inductance of the sensor coil were recorded using an impedance analyzer (WK 6505B). Because of manufacturing limitations, the titanium alloy thickness was only 0.25 mm.

Table 2. Experimental groups

ID	Stator frame	Rotor frame	Copper ring
A	yes	no	no
B	no	no	no
C	yes	yes	yes
D	no	yes	yes
E	yes	yes	no

The full range inductance gain (FRIG) of the sensor coil, an indicator of sensor sensitivity, is defined as

$$G(\omega) = \frac{L_{-0.25}(\omega) - L_{0.25}(\omega)}{L_1(\omega)}. \quad (12)$$

Figure 3 shows a comparison of the coil equivalent inductance of the stator with and without a titanium alloy frame. When the titanium alloy frame was used on the stator, the equivalent inductance of the coil decreased more rapidly and the excitation frequency increased, because the eddy current loss on the surface of the stator titanium alloy is directly proportional to the excitation frequency of the sensor coil. The excitation frequency affects the mutual inductance between the sensor coil and stator titanium alloy frame, which rises as the excitation frequency increases.

Figure 4 shows the curve of the equivalent inductance change with rotor displacement in groups C and D under excitation frequencies from 100 to 1000 kHz. When the excitation frequency was low, the gradient of the equivalent inductance with the displacement between groups C and D was approximately the same. The gradient of the equivalent

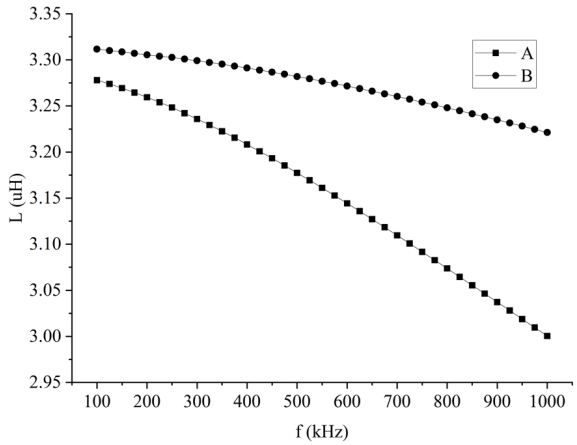

Figure 3. Comparison of equivalent inductances of groups A and B from 100 kHz to 1000 kHz

inductance became steeper with increasing excitation frequency in group D. Nevertheless, the gradient of equivalent inductance with rotor displacement changed little with increasing excitation frequency. This result shows that the titanium alloy frame on the stator weakens the sensor sensitivity.

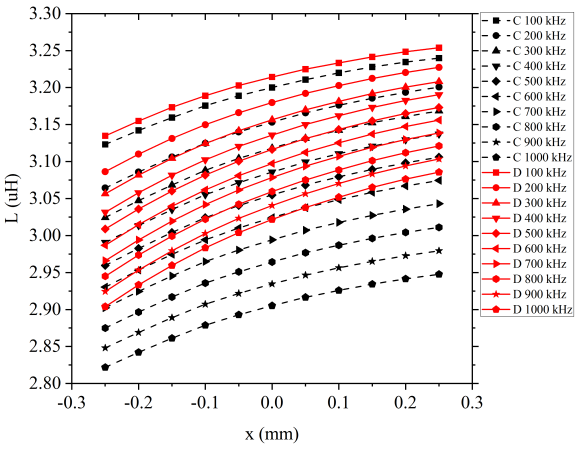

Figure 4. Equivalent inductances affected by frequency differences in groups C and group D

Figure 5 shows the resistance affected by different frequencies in group D; the equivalent resistance is inversely proportional to rotor displacement from 100 to 1000 kHz.

Figure 6 shows the equivalent resistance affected by different excitation frequencies in group C from 100 to 300 kHz, and Figure 7 shows the curve of equivalent resistance from 400 to 1000 kHz. The variation of the equivalent resistance in group C from 100 to 300 kHz is the same as that in group D, which accords with traditional regulations. Figure 7 shows that the equivalent resistance increases with increasing rotor displacement when the excitation frequency is greater than 400 kHz, which is completely contrary to the trend of equivalent resistance in conventional eddy current sensors. As the excitation frequency increases, the reversed gradient of

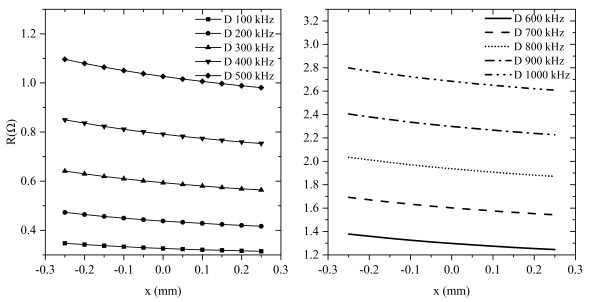

Figure 5. Equivalent resistance affected by different excitation frequencies in group D

resistance with displacement becomes significantly similar. In this case, an increase in the excitation frequency strengthens the coupling between the coil and the stator titanium alloy frame, which is compliant with the real part of Eq. (4).

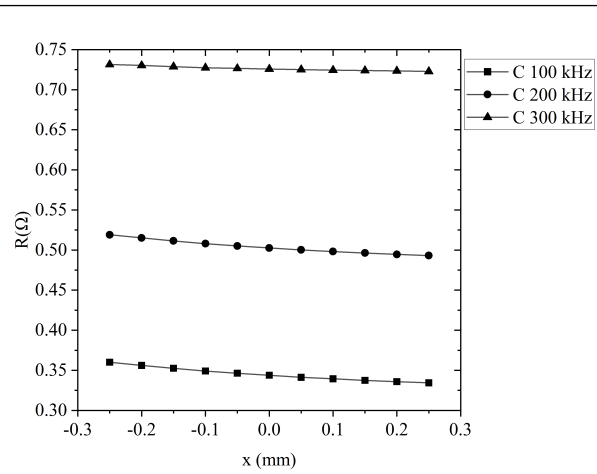

Figure 6. Equivalent resistance affected by different excitation frequencies in group C from 100 to 300 kHz

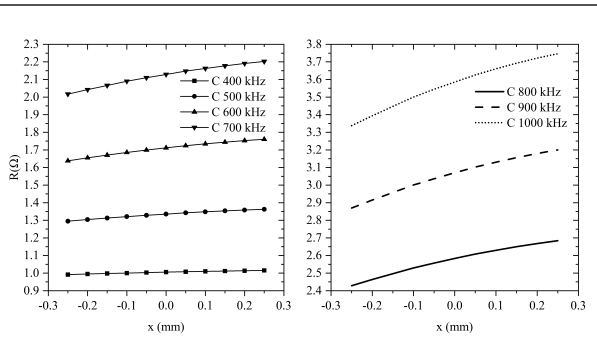

Figure 7. Equivalent resistance affected by different excitation frequencies in group C from 400 to 1000 kHz

Figure 8 shows the FRIG for different excitation frequencies in group C, D, and E. In the low-frequency band of 100–200 kHz, the curves for groups C and D exhibit minor differences in the inductance gain value. Hence, when the excitation frequency was low, the titanium alloy frame on the stator had a relatively small effect on the sensor coil, and the eddy current loss in the rotor was also small. In this condition, the sensor has low sensitivity, and its effective bandwidth is reduced, which does not benefit the dynamic response of the magnetic bearing system. Therefore, extremely or relatively low excitation frequencies are not applicable to LVADs.

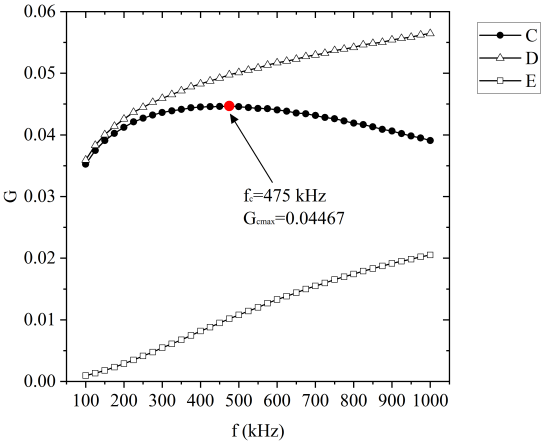

Figure 8. FRIG in groups C, D, and E with different frequencies

In group C, when the excitation frequency ranged from 100 to 475 kHz, the FRIG increased monotonically. The maximum value appeared when the excitation frequency reached 475 kHz; subsequently, the FRIG decreased while the excitation frequency continued to increase. Furthermore, when the excitation frequency exceeds 475 kHz, stator titanium alloy frames cause greater attenuation of the sensor sensitivity, which is not compensated by the sensitivity increase generated by the eddy current in the rotor. This phenomenon causes a steady decrease in sensitivity, which continues to decrease when the excitation frequency increases. In the range of 250 to 750 kHz, the FRIG remained within 5% attenuation of the maximum value. However, the attenuation of the FRIG increased to more than 12.5% of the maximum when the excitation frequency exceeded 1000 kHz. Thus, it is not beneficial for sensitivity to use an excitation frequency that is too high or too low in the presence of a stator titanium alloy frame, although a narrow range of excitation frequencies exists to choose in an actual use environment.

In group E, the FRIG monotonically increased when the excitation frequency ranged from 100 to 1000 kHz. The maximum gain value appeared at 1800 kHz frequency (not marked on the curve), and it decreased as the excitation frequency continued to increase. The maximum FRIG in group E reached only 60% of that in group C. Thus, the sensitivity is improved by adding copper beneath the titanium alloy frame in the rotor. Figure 9 shows the experimental platform.

4. Discussion

The displacement sensor in a full-maglev LVAD is vital to the system. Sensitivity and robustness directly affect the performance of the magnetic-bearing system. However, the titanium alloy frame of the pump significantly affects the impedance of the eddy current sensor. This paper proposes a

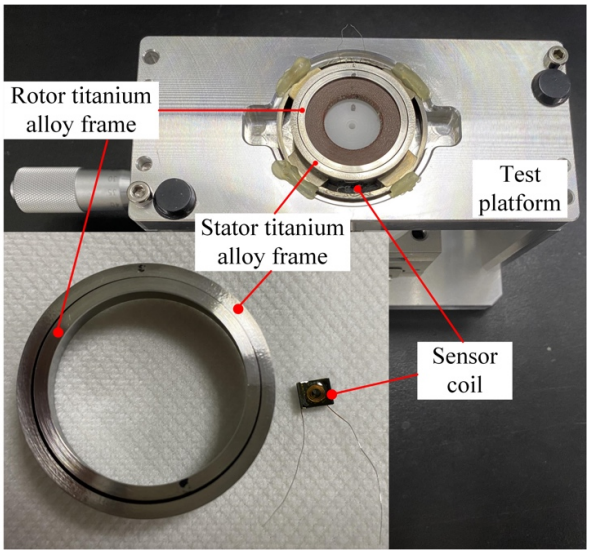

Figure 9. Experimental platform

mathematical model to demonstrate the relationship between the eddy current sensor and the titanium alloy frame. Several experiments were conducted for analysis and comparison.

The curves C and D in Figure 4 correspond to change in the imaginary part of Eq. (4) and Eq. (2), respectively. Due to the last term of the imaginary part in Eq. (4) can be guaranteed as $R_2R_3 < \omega^2 L_2 L_3$, at the same excitation frequency, the change of gradient of equivalent inductance with rotor displacement changing in group C is lower than that in group D.

According to Figures 5, 6, and 7, as the excitation frequency goes higher, when the stator is with titanium alloy frame, the variational trend of the sensor coil's equivalent resistance changing with rotor displacement varying goes to the opposite. It shows that the value of the last term of the real part in Eq. (4) is indeed greater than the sum of the two front terms as the excitation frequency increases. When the excitation frequency exceeds 400 kHz, the variational trend goes to the opposite direction.

The curve C in Figure 8 verifies the conclusion that when there is stator titanium alloy frame, as the excitation frequency goes higher, both k_{12} and k_{13} in Eq. (11) go up as well. However, the sensitivity does not monotonically increase with the excitation frequency increment. A peak value exists. That is to say, when a titanium alloy frame is used on the stator, an optimal excitation frequency exists, while higher excitation frequency does not always result in better sensitivity. This result indicates that the sensitivity is limited by the titanium alloy frame on the stator.

Comparing C and E in Figure 8 illustrates that when the rotor was embedded with high conductivity metal, k_{13} in Eq. (11) will increase, resulting in higher sensitivity, i.e., embedded copper ring under the rotor titanium alloy frame enhances the conductivity of the rotor. This property increases the sensitivity of the eddy current sensor.

The excitation frequency of the sensor directly influences its bandwidth when a titanium alloy frame is added to the stator. The designer must consider the tradeoff between sensitivity and bandwidth. With respect to the eddy current displacement sensor, whose excitation frequency is normally 500 kHz, its effective bandwidth can ensure the competency of a magnetic bearing system with 20000-rpm capacity. That characteristic is reasonable for an implantable LVAD. Alternatively, the dynamic performance of the sensor can be improved with a trade-off in sensitivity in favor of excitation frequency.

The thickness of the titanium alloy frame is limited by the manufacturing process in actual practice. The proposed model can guide designers in conducting studies and experiments to determine the optimal system frequency. However, the model cannot directly aid designers in determining the theoretical optimal frequency. This is a limitation of the mathematical model, which will be addressed in future studies.

5. Conclusion

The aim of this study was the development of mathematical models for a stator composed of a titanium alloy frame and analyses of the sensitivity of an eddy current displacement sensor applied in a full-maglev LVAD that contains a titanium alloy frame. The proposed models exhibit good universality, can be adapted to general engineering applications, and can provide better solutions to engineering designs. Experiments using different configurations the stator with titanium alloy frames and copper rings showed different equivalent inductance at different excitation frequencies and presented the relationship between equivalent resistance and rotor displacement. These results provide a theoretical basis for future LVAD upgrades.

References

[1] Oberle M., Reutemann R., Hertle R., Huang Q. A 10-mW two-channel fully integrated system-on-chip for eddy-current position sensing. IEEE Journal of Solid-State Circuits, 37(7):916–925, 2002.

[2] Fang J., Wen T. A wide linear range eddy current displacement sensor equipped with dual-coil probe applied in the magnetic suspension flywheel. Sensors (Basel, Switzerland), 12(8):10693–10706, 2012.

[3] Wang K., Zhang L., Han B., Chen S. Analysis and experiment of self-differential eddy current displacement sensor for AMBs used in molecular pump. IEEE Transactions on Instrumentation and Measurement, 67(8):1815–1824, 2018.

[4] Pai C.N., Shinshi T., Asama J., Takatani S., Shimokohbe A. Development of a compact centrifugal rotary blood pump with magnetically levitated impeller using a titanium housing. Journal of Advanced Mechanical Design Systems & Manufacturing, 2(3):345–355, 2008.

[5] Ahn C.B., Kim K.H., Moon K.C., Jeong K.S., Kim H.C., Lee J.J., Hwang C.M., Sun K. Development of eddy current sensor systems in artificial heart for noncontact gap sensing. Annual International Conference of the IEEE Engineering in Medicine and Biology Society, 4:3913–3915, 2005.

[6] Lee J.J., Chi B.A., Choi J., Park J.W., Song S.-J., Sun K. Development of magnetic bearing system for a new third-generation blood pump. Artificial Organs, 35(11):1082–1094, 2011.

[7] Sun M., Zhou J., Dong B., Zheng S. Driver circuit improvement of eddy current sensor in displacement measurement of high-speed rotor. IEEE Sensors Journal, 21(6):7776–7783, 2021.

[8] Nagaoka E., Fujiwara T., Kitao T., Sakota D., Shinshi T., Arai H., Takatani S. MedTech Mag-Lev, single-use, extracorporeal magnetically levitated centrifugal blood pump for mid-term circulatory support. Asaio Journal, 59(3):246–252, 2013.

[9] Raghunathan P., Logashanmugam E. Position servo controller design and implementation using low cost eddy current sensor for single axis active magnetic bearing. Journal of Ambient Intelligence and Humanized Computing, 10(9):3481–3492, 2019.

[10] Zhan H., Wang L., Wang T., Yu J. The influence and compensation method of eccentricity for cylindrical specimens in eddy current displacement measurement. Sensors, 20(22):6608, 2022.